Applied Catalysis B: Environmental 97 (2010) 108–114

Contents lists available at ScienceDirect

Applied Catalysis B: Environmental

journal homepage: www.elsevier.com/locate/apcatb

Sn-doped Ni/YSZ anode catalysts with enhanced carbon deposition resistance for an intermediate temperature SOFC

Hyuk Kan, Hyunjoo Lee*

Department of Chemical and Biomolecular Engineering, Specialized Graduate School of Hydrogen and Fuel Cell, Yonsei University, Sinchon-dong, Seodaemun-Gu, Seoul 120-749, Republic of Korea

ARTICLE INFO

Article history:
Received 4 January 2010
Received in revised form 12 March 2010
Accepted 23 March 2010
Available online 30 March 2010

Keywords:
Solid oxide fuel cell
Methane
Tin
Carbon resistance
Ni/YSZ

ABSTRACT

Solid oxide fuel cells (SOFCs), capable of operating in an intermediate temperature range with a high power density, are fabricated using Sn-doped Ni/YSZ as an anode catalyst with a functional layer between the anode and electrolyte. The cell shows a high power density of 0.41 W cm^{-2} at 650 °C when operated using humidified methane fuel. A comparison of this cell with a single cell prepared without Sn shows that the long-term stability is greatly improved; the Sn-doped Ni/YSZ cell operates for 137 h, whereas the Ni/YSZ cell ceases operation within 27 h. A minimal level of Sn-doping yields the best cell performance; higher levels of Sn-doping results in occupation of most catalytic active sites, causing poorer performance. In the case that carbon deposited on the Sn-doped Ni/YSZ surface during operation is removed, the long-term stability of the cell is further improved, and the cell operates stably for 300 h without degradation. The quantity and distribution of Sn on the anode surface remains nearly unchanged over the course of operation.

1. Introduction

Solid oxide fuel cells (SOFCs) convert chemical energy into electricity directly and have several advantages; they are highly efficient, fuel flexible and produce low levels of carbon emissions. Compared with other types of fuel cells, SOFCs use non-precious metal catalysts and solid electrolytes, resulting in relatively low manufacturing costs and facile operation. In addition, the current density of SOFCs is high, and waste heat generated at high operation temperatures can be used for running microturbines, further improving the overall energy efficiency of the cells [1–5].

Hydrogen, the most widely used fuel in fuel cells, is usually produced from the steam reforming of hydrocarbons. If the hydrocarbons could be used directly as a fuel, the overall energy costs would be significantly reduced [6]. SOFC anodes usually employ a cermet consisting of nickel metal and yttrium-stabilized zirconia (YSZ) for catalysts when hydrogen is used as a fuel. Use of the Ni/YSZ catalyst with hydrocarbon fuels results in deposition of large quantities of carbon on the nickel surface, resulting in a marked reduction in cell performance [7–10]. To overcome this problem, new types of catalysts, such as ceria or perovskites, have been actively investigated [11–22]. However, because SOFC manufacture is optimized for Ni/YSZ systems, it would be desirable to devise a straightforward modification of Ni/YSZ that enables cell operation using hydrocarbon fuels [23–25].

Carbon deposition occurs mainly on Ni ensembles consisting of several neighboring Ni atoms. To prevent the formation of a Ni ensemble, Ni may be alloyed with another metal [26–28]. For example, Ni–Au alloys were shown to be highly tolerant to carbon deposition when methane was used as a fuel under steam reforming conditions [29]. However, this work used a precious metal (Au) and large quantities of steam (with a methane to steam ratio of 3:1 or lower). The steam present in the fuel flow lowered the open circuit potential (OCV) significantly, and NiO formed easily on the Ni surface, reducing the number of catalytic sites. Excessive steam also degraded the overall cell stability [30–33].

In the present study, we used an inexpensive metal, Sn, for surface alloying. The anode-supported cell was fabricated using a Ni–Sn alloy, and its performance, measured by the current density and long-term stability, was tested using a humidified methane fuel. Because high-temperature SOFCs are severely restricted in terms of the choice of component material, electrode sintering and the facilitation of interfacial diffusion between the electrode and electrolyte, we targeted an intermediate range of operation temperatures (650 °C) [34,35]. To obtain a high current density at intermediate temperatures, an anode functional layer was prepared using a nanocomposite material between the bulk anode and the electrolyte [36]. The performance was then evaluated as a function of Sn added to the bulk anode or to the functional layer. The stability of Sn during cell operation was also examined.

* Corresponding author. Tel.: +82 2 2123 5759; fax: +82 2 312 6401.
E-mail address: azhyun@yonsei.ac.kr (H. Lee).

0926-3373/$ – see front matter © 2010 Elsevier B.V. All rights reserved.
doi:10.1016/j.apcatb.2010.03.029

2. Experimental

2.1. Single cell fabrication

2.1.1. Preparation of bulk anode

Sn-doped Ni/YSZ bulk anode catalysts were prepared by impregnating NiO powder (J.T. Baker) with $SnCl_2{\cdot}2H_2O$ (Aldrich, 98%) via the incipient wetness technique. Mixing of a 17.5 wt.% coarse YSZ powder (FTY 13.0-101H, Unitec Ceramics), 17.5 wt.% fine YSZ powder (TZ-8Y, Tosoh) and 65 wt.% NiO (or Sn-doped NiO) was accomplished by ball-milling in ethanol for 24 h. The catalyst was filtered and dried at 60 °C. NiO/YSZ or Sn-doped NiO/YSZ anode catalysts (90 wt.%) and carbon black forming agent (Raven 430, Columbian Chemical, 10 wt.%) were mixed by ball-milling in ethanol for 24 h, and the product was pressed at 100 MPa into a disc (~36 mm in diameter and 1.2 mm thick). The pellets were sintered at 1200 °C for 3 h in air.

2.1.2. Preparation of a functional layer

NiO/YSZ nanocomposite powders were synthesized by the Pechini method as described elsewhere [36]. Briefly, the precursors of $Ni(NO_3)_2{\cdot}6H_2O$ (Junsei Chemical Co., 99.9%), $ZrO(NO_3)_2{\cdot}xH_2O$ (Aldrich, 99.9%), $Y(NO_3)_2{\cdot}6H_2O$ (Aldrich, 99.9%) and $SnCl_2{\cdot}2H_2O$ (Aldrich, 98%) were added to distilled water and heated to around 40 °C. Next, citric acid (Junsei Chemical Co., 99.9%) and ethylene glycol (Aldrich, 99%) were added into this solution as complexation/polymerization agents at 60 °C. Next, YSZ (TZ-8YS, Tosoh) were then added to the aqueous solution. The polymeric solution condensed at 180 °C for 4 h and ash-colored intermediates were obtained. The resulting intermediates were calcined at 600 °C for 2 h and milled in ethanol to yield Sn-doped NiO/YSZ nanocomposite solution. A functional layer of the anode support was prepared by dip-coating the prepared nanocomposites, then calcining at 1200 °C for 3 h.

2.1.3. Preparation of electrolyte and cathode

YSZ (TZ-8YS, Tosoh) slurry was then applied to the functional layer via dip-coating, and the support was sintered at 1400 °C for 3 h to yield a thin, dense YSZ electrolyte layer. The cathode paste was prepared using $La_{0.8}Sr_{0.2}MnO_3$ (LSM; Praxair, 50 wt.%) and YSZ (TZ-8YS, Tosoh, 50 wt.%). The cathode layer was screen-printed on the anode-supported electrolyte with an active area of 1.5 cm^2 and a thickness of 20–30 μm. The pellet was sintered at 1150 °C for 3 h. The cell was reduced by hydrogen gas for 3 h prior to cell operation.

2.2. Characterization of the anode catalysts

The Sn-doped Ni/YSZ anode catalyst was characterized using X-ray diffraction (XRD) and scanning electron microscopy (SEM). Powder XRD patterns were recorded on a Rigaku Muniflex X-ray diffractometer using Cu/Kα radiation at a tube voltage of 30 kV and a tube current of 15 mA, with a scan speed of 2° min^{-1}. SEM analysis was performed using a Jeol 6500F (15 kV) microscope equipped with an EDX analytic system. SEM/EDX was used to examine the samples before and after cell operation. The carbon deposits on the samples were analyzed using temperature-programmed oxidation (TPO) by raising the temperature at a heating rate of 10 °C min^{-1}, from room temperature to 900 °C, under a flowing stream of 10% O_2 in He (30 ml min^{-1}). The outflowing gases were detected by thermal conductivity detector (TCD). The quantity of Sn in the cell was measured using an inductively coupled plasma (ICP) atomic emission spectrophotometer (IRIS Intrepid II XSP, Thermo).

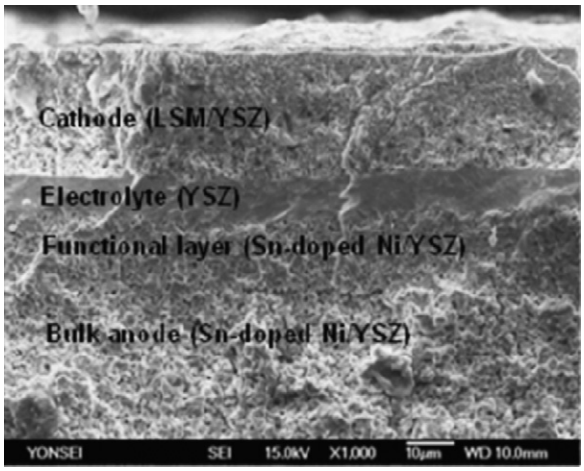

Fig. 1. SEM images of a cross-sectional area of an anode-supported Sn-doped Ni/YSZ single cell with a functional layer (1Anode/1FL). 1Anode means that 1 wt.% (with respect to Ni) of Sn was used for anode fabrication and 1FL means that 1 wt.% (with respect to Ni) of Sn was used for anode functional layer fabrication.

2.3. Cell-testing

Cell performances of the anode-supported single cells were evaluated at 650 °C under humidified hydrogen (200 cm^3 min^{-1}, 3% H_2O) or humidified methane (100 cm^3 min^{-1}, 3% H_2O) on the anode side, and with air (300 cm^3 min^{-1}) on the cathode side. The employed cell-testing equipment is described elsewhere [37]. A Pt mesh (Alfa) was used as a current collector on the cathode side, and Au felt was used on the anode side. *I–V* characterization, durability and electrochemical impedance spectra were measured using a Solartron 1260 frequency analyzer and a Solartron 1287 interface. In the impedance test, the frequency ranged from 0.1 Hz to 10 kHz, with signal amplitude of 10 mV. Regeneration of the fuel cell was accomplished using air for the oxidative removal of deposited carbon. Air was delivered to the anode surface with a flow rate of 50 cm^3 min^{-1} at 650 °C for 1 h. Subsequently, the anode was fully reduced under an H_2 atmosphere at 650 °C for 5 h, prior to the next round of cell operation.

3. Results and discussion

3.1. Microstructure of the Sn-doped Ni/YSZ anode

SOFC single cells were fabricated using Sn-doped Ni/YSZ as the anode catalyst. A functional layer was added between the electrolyte and the bulk anode to minimize the interfacial resistance. The functional layer is known to produce more three phase-boundary points, which are true reactive sites [36]. Fig. 1 shows a cross-sectional SEM image of an anode-supported fuel cell with a Sn composition of 1Anode/1FL, where 1Anode denotes 1 wt.% Sn (with respect to Ni) added during the bulk anode catalyst synthesis, and 1FL denotes 1 wt.% Sn (with respect to Ni) added during the functional layer synthesis. For comparison, both Ni/YSZ and Sn-doped Ni/YSZ single cell were prepared. The bulk anode catalysts yielded the same XRD pattern for both Ni/YSZ and Sn-doped Ni/YSZ as shown in Supplementary data, Fig. S1, indicating that the minimal quantity of Sn added during fabrication did not form a distinct phase.

Many calcination steps were required during the cell fabrication procedure, with temperatures as high as 1400 °C. To check the distribution of Sn after treatment under such harsh conditions, we performed EDX mapping for Ni and Sn in both the functional layer and bulk anode regions. Ni and Sn distributions were measured at

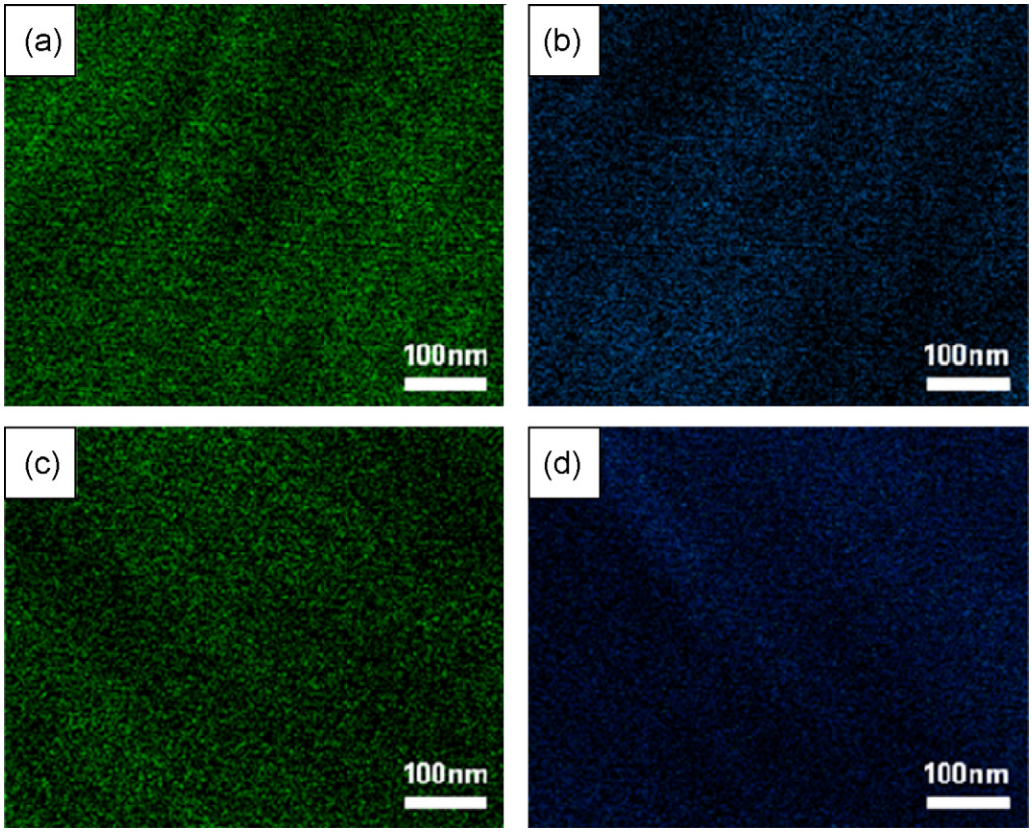

Fig. 2. EDX images of Sn-doped Ni/YSZ fuel cell (1Anode/1FL): bulk anode showing (a) Ni, (b) Sn and the functional layer showing (c) Ni, (d) Sn distribution.

the same position in the sample. As shown in Fig. 2, Ni and Sn were uniformly distributed on the surface. For the 1Anode/1FL anode catalyst, the Sn content was measured by EDX to be 4.5 wt.% in the functional layer and 18.3 wt.% in the bulk anode. Sn remained preferentially on the surface of the Ni–Sn alloy, in agreement with previous reports [38]. In particular, a higher quantity of Sn was observed on the bulk anode surface, which was prepared by impregnating the NiO surface with Sn salts, than on the functional layer, which was synthesized by calcining both Ni and Sn salts.

3.2. Single cell tests

The performances of the single cells were measured using humidified (3% H_2O) methane as a fuel. Fig. 3(a) compares the *I–V* curves for Ni/YSZ and Sn-doped Ni/YSZ single cells. The current density profiles are similar, with a maximum power density of 0.39 W cm^{-2} for Ni/YSZ and 0.41 W cm^{-2} for Sn-doped Ni/YSZ. The cell performances of a 1Anode/1FL Sn-doped Ni/YSZ single cell at various operation temperatures are shown in Fig. 3(b). The maximum power densities are 1.01 W cm^{-2} at 800 °C, 0.68 W cm^{-2} at 700 °C and 0.41 W cm^{-2} at 650 °C. The electrochemical impedances were also tested for Ni/YSZ and Sn-doped Ni/YSZ single cells. The impedance spectra were identical for both cases as shown in Supplementary data, Fig. S2, implying that Sn has little influence on the electrochemical impedance. The long-term stability of the cell was evaluated at 650 °C when 0.3 A cm^{-2} of current density was loaded. As demonstrated in Fig. 4, the 1Anode/1FL Sn-doped Ni/YSZ cell operated stably for >120 h, then ceased operation at 137 h. In contrast, when no Sn was added, the cell degraded rapidly and ceased operation at 27 h. These results confirm that the long-term stability could be significantly enhanced by the addition of a minimal quantity of Sn to the Ni/YSZ anode catalyst. Recently,

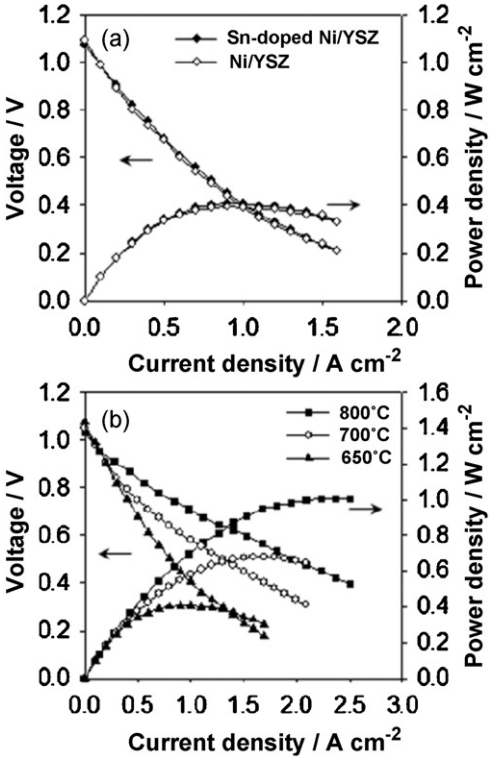

Fig. 3. (a) *I–V* curves measured at 650 °C for Ni/YSZ and Sn-doped Ni/YSZ (1Anode/1FL) single cells and (b) *I–V* curves measured at various temperatures for Sn-doped Ni/YSZ (1Anode/1FL) under humidified methane flow.

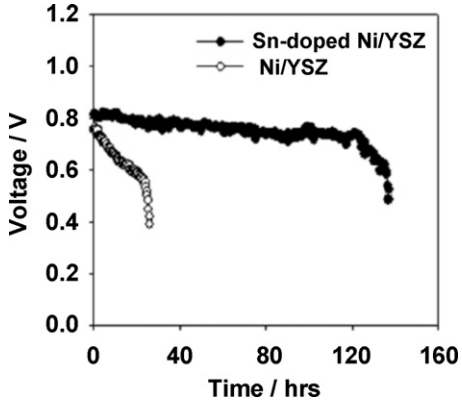

Fig. 4. Long-term stability tests measured at 650 °C. Applied load of current density was 0.3 A cm^{-2} and humidified methane was used as a fuel.

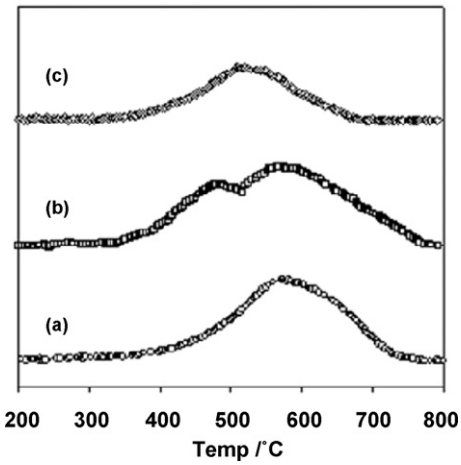

Fig. 5. Temperature-programmed oxidation results for (a) Ni/YSZ after the cell stopped in 27 h, (b) Sn-doped Ni/YSZ (1Anode/1FL) after the cell stopped in 137 h and (c) Sn-doped Ni/YSZ (1Anode/1FL) after the cell operated stably for 50 h. The fuel cells were operated at 650 °C under humidified methane flow.

other group also reported that Sn/Ni alloy SOFC anode exhibits good carbon tolerance in the hydrocarbon fuels [39].

3.3. Carbon deposition on the anodes

When the oxidation of methane occurred at the Ni surface, large quantities of cokes were observed. In particular, fibrous carbon deposits were produced at 650 °C [40]. The nucleation and growth of these cokes could be hindered by alloying Ni with other metals, because the alloying reduces the number of Ni atom ensembles, which are essential for coke formation.

Fig. 5 shows features of the carbons deposited onto the Ni/YSZ or Sn-doped Ni/YSZ single cell (1Anode/1FL), investigated by TPO for the anode catalyst in the Ni/YSZ cell which ceased operation at 27 h (Fig. 5(a)), the Sn-doped Ni/YSZ cell which ceased operation at 137 h (Fig. 5(b)), or the Sn-doped Ni/YSZ which operated stably for 50 h (Fig. 5(c)). Ni/YSZ showed a single peak at 572 °C and Sn-doped Ni/YSZ showed a single peak at 508 °C under stable operation. However, Sn-doped Ni/YSZ showed two peaks at 476 and 568 °C after the cell ceased operation, respectively.

The TPO results indicate the presence of two types of carbon. According to the XRD results for these anode catalysts (Supplementary data, Fig. S2), a graphite peak was observed at 26.8° for both Ni/YSZ and Sn-doped Ni/YSZ after the cells ceased operation. In contrast, the Sn-doped Ni/YSZ cell, under stable operation, did not yield a graphite peak. Therefore, the carbon present on the stopped cells was found to be crystalline graphitic in form, and the carbon present on the Sn-doped Ni/YSZ, under stable opera-

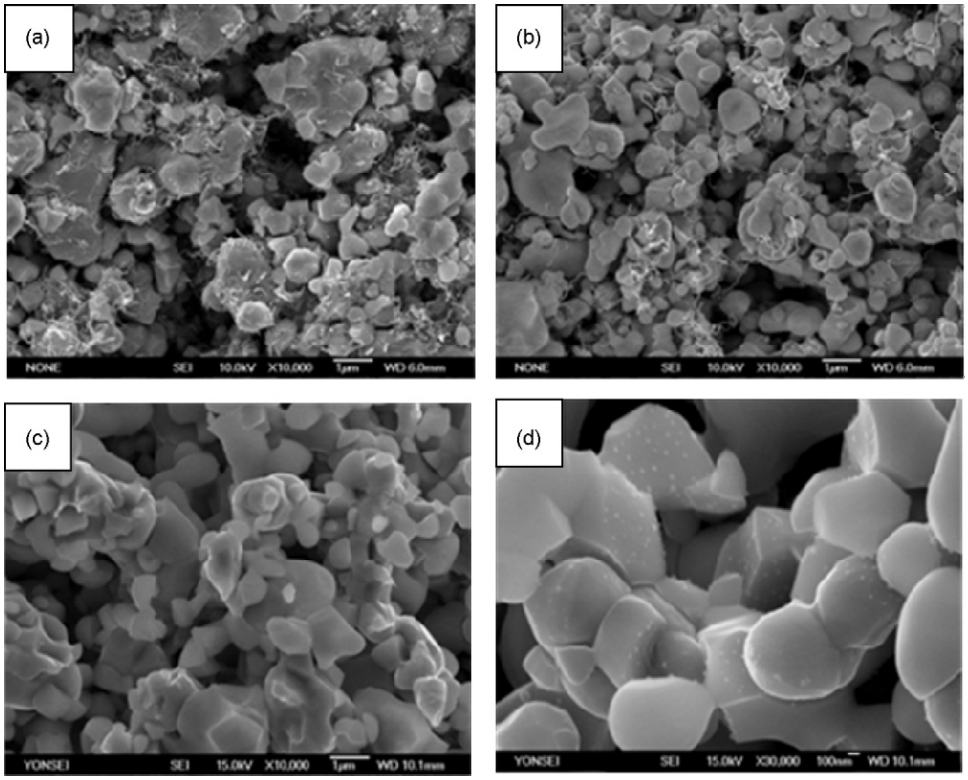

Fig. 6. SEM images of the anode over (a) Ni/YSZ, (b) Sn-doped Ni/YSZ (1Anode/1FL) after the cell stopped and (c and d) Sn-doped Ni/YSZ (1Anode/1FL) after the cell operated for 50 h at 650 °C.

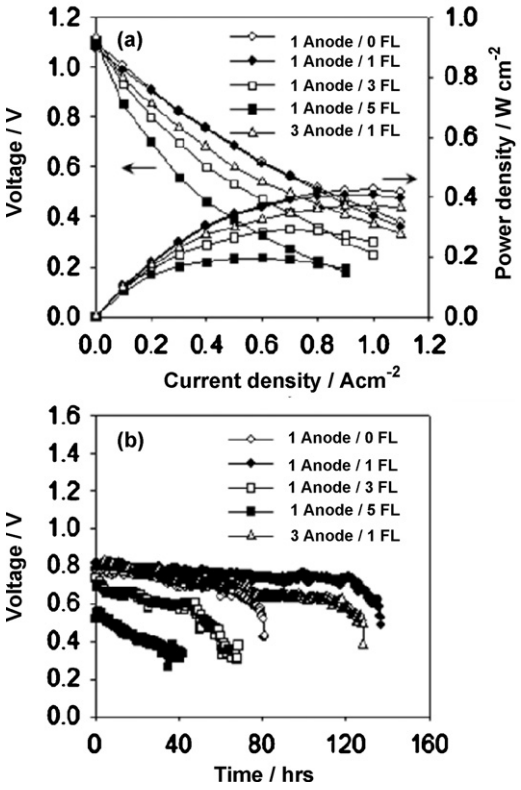

Fig. 7. Cell performance tests for various amounts of Sn on anode catalysts: (a) *I–V* curves, (b) long-term stability results. Applied load of current density was 0.3 A cm^{-2}. The fuel cells were operated at 650 °C under humidified methane.

tion, was amorphous in form. The carbon atoms that were oxidized at higher temperatures during TPO were graphitic, and the carbon atoms oxidized at lower temperatures were amorphous. The amorphous carbons appeared to form at an early stage of cell operation. As the carbons were accumulated, amorphous carbons transformed into graphitic carbon, destroying the integrated structure of the single cell. Fig. 6 shows the morphology of the deposited carbon under the three conditions described. Many fibrous carbon deposits were observed after the cells ceased operation, but the Sn-doped Ni/YSZ cell, under stable operation, rarely presented fibrous carbon atoms. The deposition of fibrous crystalline carbon appeared to be the cause of cell degradation. Carbon crystallization on Sn-doped Ni/YSZ occurred much more slowly, enhancing the long-term stability of the fuel cell.

The electrochemical impedance spectra also confirmed the formation of different types of carbons on the anodes. The overall electrode polarization resistance increases with time on Ni/YSZ anode while it decreases with time on Sn-doped Ni/YSZ anode as shown in Supplementary data, Fig. S4. The crystalline graphitic carbons deform the cell, increasing the electrode polarization resistance. On the other hand, the amorphous carbons deposited on Sn-doped Ni/YSZ rather decrease the electrode polarization resistance probably due to enhanced electron conductivity as reported previously [13].

3.4. Effect of Sn quantity on cell performance

The dependence of cell performance on Sn content was evaluated. The Sn content present in the functional layer region, as a function of the quantity of Sn added during synthesis of the functional layer, was measured by EDX. For the 1 wt.% (1FL), 3 wt.% (3FL) and 5 wt.% (5FL) additions of Sn to the functional layer, the measured quantities of Sn increased proportionally, yielding 4.5, 12.8 and 20.4 wt.%, respectively. Fig. 7 shows the single cell performance for varying Sn content. For a bulk anode with 1 wt.% Sn (1Anode), the maximum power density decreased to 0.43, 0.41, 0.29 and 0.20 W cm^{-2} as the Sn content in the functional layer increased to 0, 1, 3 and 5FL, respectively. Although 0FL and 1FL showed similar performances, the power density decreased significantly as the Sn content increased. An excess of Sn on the surface reduced the number of catalytically active sites, generating the decreased power density.

Table 1
The amounts of Sn measured before the cell operates and after the cell ceases operating. The numbers in the table show Sn weight percentage measured by ICP.

	Before operating (wt.%)	After shutting down (wt.%)
1Anode/0FL	0.98	0.94
1Anode/1FL	1.25	1.17
1Anode/3FL	1.65	1.56
1Anode/5FL	1.93	1.88
3Anode/1FL	2.85	2.67

The long-term stability of the cells was tested for cells prepared with varying quantities of Sn. The voltage was measured over the course of a long operation time using humidified methane as a fuel under a current density of 0.3 A cm^{-2}. Cells ceased operation at 81, 137, 68 and 42 h for the 1Anode/0FL, 1Anode/1FL, 1Anode/3FL and 1Anode/5FL cells, respectively. When the Sn content in the bulk anode was increased to 3 wt.% (3Anode) for 1FL, the operation time was 129 h. The above results demonstrate that the 1Anode/1FL cell showed the best power density and long-term stability. The formation of a Ni–Sn alloy appeared to be very effective for minimizing carbon deposition on the Ni surfaces. However, excessive Sn diminished the cell performance via occupation of a majority of the reactive sites.

3.5. Stability of Sn

The Sn content was evaluated both before and after cell operation. Cells became fragile after ceasing operation, such that it was difficult to distinguish the functional layer region from the bulk anode region. Therefore, the Sn content was measured over the entire anode region by ICP. The deposited carbon was removed by incineration under air at 800 °C for 2 h. The change in Sn content as a result of cell operation is shown in Table 1. Regardless of the length of cell operation, 94–97% of the initially present Sn remained after operation. The Sn appeared to be stable even after many hours of cell operation. If carbon deposition was excessive, the carbon turned into crystalline graphite, destroying the cell's stability. This

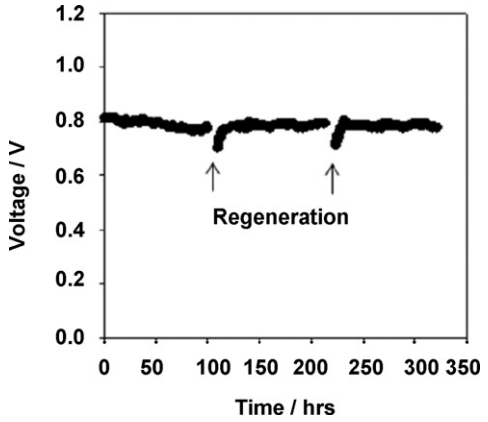

Fig. 8. Long-term stability test measured at 650 °C. Applied load of current density was 0.3 A cm^{-2} and humidified methane was used as a fuel. Air was flowed in the anode side for an oxidative removal of carbon deposits every 100 h of cell operation.

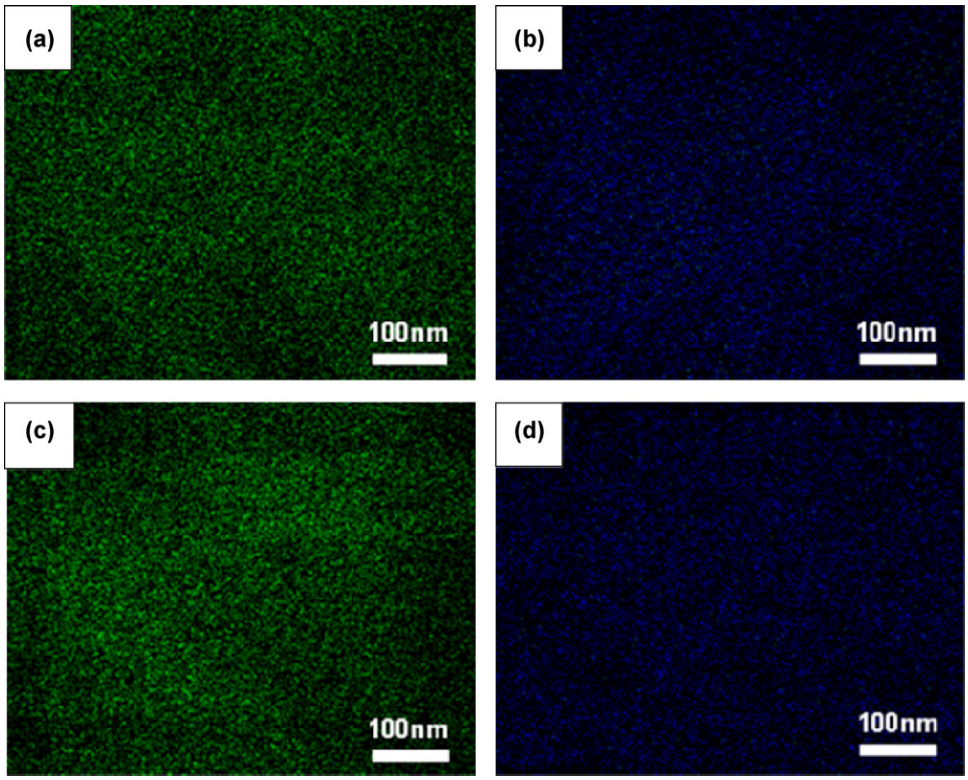

Fig. 9. EDX images of Sn-doped Ni/YSZ fuel cell (1Anode/1FL) after the cell operated for 300 h: bulk anode showing (a) Ni, (b) Sn and the functional layer showing (c) Ni, (d) Sn distribution.

problem could be solved by removing the carbon deposits before they transformed into graphite.

Fig. 8 shows the performance of a cell that was operated stably for 100 h, intentionally stopped, then subjected to incineration in air to burn away the deposited carbon. The cell was then restarted and allowed to operate after reduction of the catalysts. This regeneration procedure was repeated twice. The cell operated stably for 300 h without observed degradation. The Sn distribution was examined by EDX mapping after 300 h of operation. The deposited carbons were removed by the calcination procedure, as described earlier. As demonstrated in Fig. 9, Sn was distributed uniformly on the Ni surface. The Sn content, measured by EDX, was 5.2 wt.% in the functional layer and 17.2 wt.% in the bulk anode. The change in Sn content was negligible after 300 h of operation. The above results confirm that Sn was stable on the Ni surface despite many hours of operation.

4. Conclusions

Sn-doped Ni/YSZ was used as an anode catalyst for SOFC single cell fabrication. To obtain a high power density at intermediate temperatures, a functional layer was added between the bulk anode and the electrolyte. For single cells with the same microstructure, Ni/YSZ and Sn-doped Ni/YSZ showed similar power densities (0.39 W cm^{-2} vs. 0.41 W cm^{-2}), but Sn-doped Ni/YSZ showed enhanced long-term stability (27 h vs. 137 h). The stability resulted from a much lower rate of deposition of amorphous carbon. The effect of Sn content on cell performance was evaluated by varying the amount of Sn used during cell fabrication. Whereas a minimal quantity of Sn enhanced cell performance significantly, the enhancement decreased as the quantity of Sn increased. Because Sn preferentially remained on the surface, the presence of excess Sn resulted in occupation of a high proportion of surface active sites, diminishing the anodic reaction. When the carbon deposited on the Sn-doped Ni/YSZ single cell was removed during operation, the cell operated stably for 300 h without observed degradation. This finding confirms that the Sn present on the anode surface was stable despite many hours of operation. This work can be a good practical solution to use Ni/YSZ system for methane fuel with a minimal modification.

Acknowledgement

This work was supported by DAPA/ADD of Korea, the Seoul R&BD Program (CS070157) and New & Renewable Energy R&D program (2009T100100606) under the Ministry of Knowledge Economy of Korea.

Appendix A. Supplementary data

Supplementary data associated with this article can be found, in the online version, at doi:10.1016/j.apcatb.2010.03.029.

References

[1] A. Atkinson, S. Barnett, R.J. Gorte, J.T.S. Irvine, A.J. Mcevoy, M. Mogensen, S.C. Singhal, J. Vohs, Nat. Mater. 3 (2004) 17–27.
[2] E.P. Murray, T. Tsai, S.A. Barnett, Nature 400 (1999) 649–651.
[3] A.B. Stambouli, E. Traversa, Renew. Sust. Energy Rev. 6 (2002) 433–455.
[4] S.W. Tao, J.T.S. Irvine, Nat. Mater. 2 (2003) 320–323.
[5] Z.L. Zhan, S.A. Barnett, Science 308 (2005) 844–847.
[6] J.N. Armor, Appl. Catal. A: Gen. 176 (1999) 159–176.
[7] C.M. Finnerty, N.J. Coe, R.H. Cunningham, R.M. Ormerod, Catal. Today 46 (1998) 137–145.
[8] Y.B. Lin, Z.L. Zhan, J. Liu, S.A. Barnett, Solid State Ionics 176 (2005) 1827–1835.
[9] K. Nikooyeh, R. Clemmer, V. Alzate-Restrepo, J.M. Hill, Appl. Catal. A: Gen. 347 (2008) 106–111.
[10] H. Timmermann, W. Sawady, D. Campbell, A. Weber, R. Reimert, E. Ivers-Tiffee, J. Electrochem. Soc. 155 (2008) B356–B359.
[11] M. Asamoto, S. Miyake, K. Sugihara, H. Yahiro, Electrochem. Commun. 11 (2009) 1508–1511.

[12] B. Mosqueda, J. Toyir, A. Kaddouri, P. Gelin, Appl. Catal. B: Environ. 88 (2009) 361–367.
[13] H. Kim, C. Lu, W.L. Worrell, J.M. Vohs, R.J. Gorte, J. Electrochem. Soc. 149 (2002) A247–A250.
[14] D. La Rosa, A. Sin, M. Lo Faro, G. Monforte, V. Antonucci, A.S. Arico, J. Power Sources 193 (2009) 160–164.
[15] S.I. Lee, J.M. Vohs, R.J. Gorte, J. Electrochem. Soc. 151 (2004) A1319–A1323.
[16] M. Lo Faro, D. La Rosa, I. Nicotera, V. Antonucci, A.S. Arico, Appl. Catal. B: Environ. 89 (2009) 49–57.
[17] S.D. Park, J.M. Vohs, R.J. Gorte, Nature 404 (2000) 265–267.
[18] P. Tsiakaras, C. Athanasiou, G. Marnellos, M. Stoukides, J.E. ten Elshof, H.J.M. Bouwmeester, Appl. Catal. A: Gen. 169 (1998) 249–261.
[19] N. Laosiripojana, S. Assabumrungrat, Appl. Catal. B: Environ. 60 (2005) 107–116.
[20] E. Ramirez-Cabrera, A. Atkinson, D. Chadwick, Appl. Catal. B: Environ. 47 (2004) 127–131.
[21] S. Zhao, R.J. Gorte, Appl. Catal. A: Gen. 277 (2004) 129–136.
[22] N. Laosiripojana, S. Assabumrungrat, Appl. Catal. B: Environ. 82 (2008) 103–113.
[23] E. Kendrick, M.S. Islam, P.R. Slater, J. Mater. Chem. 17 (2007) 3104–3111.
[24] F.M.B. Marques, V.V. Kharton, Ionics 11 (2005) 321–326.
[25] F. Zhao, A.V. Virkar, J. Power Sources 141 (2005) 79–95.
[26] E. Nikolla, J. Schwank, S. Linic, J. Catal. 263 (2009) 220–227.
[27] T. Takeguchi, R. Kikuchi, T. Yano, K. Eguchi, K. Murata, Catal. Today 84 (2003) 217–222.
[28] D.L. Trimm, Catal. Today 49 (1999) 3–10.
[29] I. Gavrielatos, V. Drakopoulos, S.G. Neophytides, J. Catal. 259 (2008) 75–84.
[30] T.J. Huang, M.C. Huang, J. Power Sources 168 (2007) 229–235.
[31] Y.S. Seo, A. Shirley, S.T. Kolaczkowski, J. Power Sources 108 (2002) 213–225.
[32] H. Timmermann, D. Fouquet, A. Weber, E. Ivers-Tiffee, U. Hennings, R. Reimert, Fuel Cells 6 (2006) 307–313.
[33] J.M. Klein, M. Henault, C. Roux, Y. Bultel, S. Georges, J. Power Sources 193 (2009) 331–337.
[34] K.Q. Huang, R.S. Tichy, J.B. Goodenough, J. Am. Ceram. Soc. 81 (1998) 2565–2575.
[35] T. Ishihara, H. Matsuda, Y. Takita, J. Am. Chem. Soc. 116 (1994) 3801–3803.
[36] S.D. Kim, H. Moon, S.H. Hyun, J. Moon, J. Kim, H.W. Lee, J. Power Sources 163 (2006) 392–397.
[37] S.D. Kim, H. Moon, S.H. Hyun, J. Moon, J. Kim, H.W. Lee, Solid State Ionics 177 (2006) 1389–1390.
[38] E. Nikolla, J. Schwank, S. Linic, J. Catal. 250 (2007) 85–93.
[39] E. Nikolla, J. Schwank, S. Linic, J. Electrochem. Soc. 156 (2009) B1312–B1316.
[40] H.P. He, J.M. Hill, Appl. Catal. A: Gen. 317 (2007) 284–292.